Biosensors and Bioelectronics 148 (2020) 111794

Contents lists available at ScienceDirect

Biosensors and Bioelectronics

journal homepage: http://www.elsevier.com/locate/bios

Non-lytic M13 phage-based highly sensitive impedimetric cytosensor for detection of coliforms

Mohammed Sedki [a], Xingyu Chen [b], Chuan Chen [b], Xin Ge [b], Ashok Mulchandani [b,*]

[a] Department of Materials Science and Engineering, University of California, Riverside, CA, 92521, USA
[b] Department of Chemical and Environmental Engineering, University of California, Riverside, CA, 92521, USA

ARTICLE INFO

Keywords:
M13 phage
Non-lytic
Fecal coliforms
Impedimetric
E. coli
Biosensor

ABSTRACT

A highly sensitive and selective non-lytic *M13* phage-based electrochemical impedance spectroscopy (EIS) cytosensor for early detection of coliforms is introduced for the first time. Gold nanoparticles were electrochemically deposited on the surface of glassy carbon electrode, and the M13 phage particles were immobilized on them using 3-mercaptopropionic acid linker and zero-length crosslinking chemistry (EDC/NHS). Next, the sensor surface was blocked to avoid non-specific binding. The M13-EIS cytosensor was tested for detection of F^+ pili *Escherichia coli species*, using *XL1-Blue* and *K12* strains, as examples of coliforms. The selectivity against non-host strains was demonstrated using *Pseudomonas Chlororaphis*. The binding of *E. coli* to the *M13* phage on the cytosensor surface increased the charge transfer resistance, enabling detection of coliforms. The biosensor achieved a limit of detection (LOD) of 14 CFU/mL, the lowest reported to-date using EIS-phage sensors, and exhibited a high selectivity towards the tested coliforms. The SEM micrographs confirmed the successful capturing of *E. coli* on the M13-based EIS cytosensor. Moreover, the sensor showed almost the same sensitivity in the simulated river water samples as in phosphate buffer, reflecting its applicability to real samples. On the other hand, this sensor system exhibited high stability under harsh environmental conditions of pH (3.0–10.0) and temperature as high as 45 °C for up to two weeks. Overall, this sensor system has excellent potential for real field detection of fecal coliforms.

1. Introduction

Bacterial infectious diseases remain one of the main causes of morbidity and mortality worldwide. Around 250 million people, per year, are affected by pathogenic infections, of which around 8% are mortal (Dye, 2014). Although there is a progress in reducing the number of deaths caused by bacterial infections, it is only by 1%. Fecal coliform contamination in aquatic environments is a serious problem, caused mainly by the presence of human or animal fecal material in water (Wibowo et al., 2018). Fecal coliforms cause diarrhea, but they are not highly pathogenic by their nature. However, large number of fecal coliforms in water indicate the higher risk of the presence of other pathogens in water, causing severe infections, including dysentery, typhoid fever, ear infections, hepatitis A, etc. *Escherichia coli* is considered the main indicator of fecal contaminations used in the water quality testing (Ashbolt et al., 2001; Massad-Ivanir et al., 2016; Odonkor and Ampofo, 2013).

The currently available diagnostic tools for coliform use complex and time-consuming microbiological assays such as selective growth, cell counting, microscopic examination, etc. (Spiegelman et al., 2005; Keer and Birch, 2003). Moreover, the results from these techniques are also hard to interpret and need expertise. Other contemporary techniques such as ELISA (Byrne et al., 2009) and PCR (v. Wintzingerode et al., 1997) are used with high sensitivity for detection of microbes. However, they are also expensive and time-consuming (Hassan and Wollenberger, 2016; Lim et al., 2005).

Recently, microbial electrochemical sensors (MESs) were introduced as accurate, real-time and highly sensitive systems for early detection of microbes, assessment of cell viability, and understanding the biochemical pathways and mechanisms (Rawson et al., 2014; Sedki et al., 2017; Selim et al., 2017; Wallace et al., 2010). Electrochemical biosensors attract great deal of attention because they are fast and highly sensitive (Bao et al., 2013; Ivnitski et al., 2000; Setterington and Alocilja, 2012; Zhang et al., 2018). Electrochemical impedance spectroscopy (EIS) is an effective tool to rapidly and sensitively monitor the minute changes at the electrode interface. Moreover, EIS is a nondestructive technique due

* Corresponding author.
E-mail address: adani@engr.ucr.edu (A. Mulchandani).

https://doi.org/10.1016/j.bios.2019.111794
Received 10 September 2019; Received in revised form 8 October 2019; Accepted 17 October 2019
Available online 22 October 2019

to the small amplitude perturbation (Guo et al., 2011). Therefore, the label-free electrochemical impedance cytosensors have been increasingly explored for clinical diagnosis (Han et al., 2016).

The specificity of a biosensor for a specific detection of a target bacteria/microorganism greatly depends on the type of the biorecognition element. In this regard, aptamers, peptides, and antibodies possess high selectivity. However, they are highly sensitive to the environmental conditions and susceptible to damage or loss of binding activity in harsh conditions (Zhou et al., 2017). On the other hand, bacteriophages, or shortly phages, are viruses that bind very strongly and specifically to target bacteria (Chen et al., 2015b; Soper et al., 2002; Zhou et al., 2017). Phages have many advantages that entitle them to be heavily used as biorecognition elements (Chen et al., 2015b). Phages are inexpensive and easy to prepare and purify, stable in harsh conditions of organic solvents and high temperature (Chen et al., 2015b; Ertürk and Lood, 2018; Handa et al., 2008; Janczuk et al., 2016; Nanduri et al., 2007). Moreover, phages are easy to immobilize on sensor surface due to their functional groups (Janczuk et al., 2016).

The phage recognizes its host bacterium through binding to specific receptors on the bacterial surface. Upon attachment, the phage penetrates the bacterial cell membrane, injects its genetic material (DNA/RNA) that initiates protein synthesis, replication and phage assembly inside the bacterium (Edgar et al., 2006). The phages then exit bacterial cell by different mechanisms depending on the type of the phage; either by cell lysis (lytic phages), such as T4 & T7 phages, or by extrusion without killing the host cell (non-lytic phage), for example M13 phage (Ploss and Kuhn, 2010).

Zhou et al. (2017) used T2 bacteriophage-based biosensor for electrochemical detection of *E. coli* B, with a limit of detection of 10^3 CFU/mL. The sensor's first response was an increase in impedance due to the attachment of the insulating layer of bacteria, followed by a sudden decrease due to the release of molecules on cell lysis. This makes the biosensor less reliable, if more bacteria were still getting immobilized while others are being ruptured, producing opposite responses. Other studies used the lytic phages (λ, T4 & T7) for cell lysis to release some molecules, such as β-galactosidase, which were used indirectly in the qualitative and quantitative detection of bacteria (Burnham et al., 2014; Chen et al., 2015a; Neufeld et al., 2003). Although the low detection limit of a few CFU was achieved by detecting the released molecules, the detection required a very long time (6 h).

In this work, we present for the first time, a non-lytic filamentous M13 phage-modified impedimetric microbial biosensor for an early detection of the fecal coliform bacteria, *E. coli*. When compared to reported cytosensors using lytic phages where the sensor response initially increased due to bacteria attachment and then decreased due to release of conductive cellular contents upon cell lysis, the response of our sensor only increased with increasing concentration/binding of *E. coli* to non-lytic *M13* phage. This we believe is an advantage. The *M13* phage is immobilized on the electrodeposited gold nanoparticles (AuNPs) on glassy carbon electrode (GCE) by means of covalent bonding using 3-mercaptopropionic acid as a linker between AuNPs and M13. The limit of detection of the biosensor is very promising, reaching the LOD of 14 CFU/mL, and the sensor has excellent stability over a wide range of pH (3.0–10.0) and temperatures (25 and 45 °C) for up to two weeks.

2. Materials and methods

2.1. Materials

Gold chloride hydrate, potassium ferricyanide, 3-mercaptopropionic acid (MPA), 2-(N-morpholino) ethane sulfonic acid (MES), 1-Ethyl-3-(3-dimethylaminopropyl) carbodiimide (EDC), N-Hydroxysuccinimide (NHS), and Bovine serum albumin (BSA) were purchased from Sigma-Aldrich (St. Louis, USA). Ethanol amine (EA) was purchased from Acros Organic-Fisher Scientific. All solutions were prepared with Milli-Q water.

2.2. Cell culture and bacteriophage preparation

Single colony of *E. coli* XL1-blue (or *E. coli* K12) was inoculated to LB media supplemented with 10 μg/mL tetracycline and incubated at 37 °C with 250 rpm shaking. After overnight culture, cells were harvested by centrifugation at 5,000×g for 5 min. Collected cells were washed three times with PB buffer and ready for assays. Similarly, *Pseudomonas chlororaphis* was cultured in LB media.

For bacteriophage preparation, overnight culture of XL1-blue was 1:100 inoculated to 50 mL 2 × YT/Tet media and cultured at 37 °C with shaking. When OD_{600} reached 0.3, 100 μL stock of bacteriophage M13KO7 ($\sim 10^{13}$ pfu/mL) was added to cell culture and incubated at 37 °C without shaking for 30 min. Kanamycin was then added to media to give a final concentration of 35 μg/mL. Cells were overnight cultured at 30 °C, 250 rpm, and centrifuged at 7,000×g for 30 min. The supernatant was collected and mixed with 12.5 mL ice-cold 20% w/v PEG6000/2.5 M NaCl solution. After incubation for 2 h at 4 °C, the mixture was centrifuged at 11,000 ×g for 30 min and the pellets were resuspended in 10 mL TE (10 mM Tris/1 mM EDTA). The resuspended solution was centrifuged at 18,000 ×g for 15 min and the supernatant was filtered by using 0.22 μm filters. The titer of prepared phage was determined by serial dilution of infected XL1-blue cells on Tet/Kan agar plates.

2.3. Electrodeposition of AuNPs

Before electrodeposition of AuNPs on its surface, GCE (3 mm in diameter) was polished with 0.2 μm alumina slurry on microcloth pad, rinsed and washed ultrasonically with deionized water. AuNPs were electrochemically deposited on the cleaned GCE by 15 cycles of cyclic voltammetry (CV) in 10 mM gold chloride solution by scanning the potential from −0.7 to −1.2 V at a scan rate of 0.05 V/s (Elias et al., 2012). Pt mesh worked as the counter electrode, while Ag/AgCl was used as the reference electrode. The prepared AuNPs were characterized by SEM imaging, EDX spectroscopy, CV and EIS measurements. The SEM FEI NNS450 was used in all SEM characterizations in this work.

2.4. Surface modification with M13 phage

Fig. 1 shows a schematic of the surface modification steps, including electrodeposition of AuNPs, for sensor fabrication. GCE with electrodeposited AuNPs was immersed in 0.1 M solution of MPA in ethanol for 1 h to form a self-assembled monolayer on gold surface, followed by washing with ethanol to remove any physically adsorbed MPA molecules. The carboxyl group of MPA was then activated using EDC/NHS chemistry. Briefly, the Au-MPA electrode was immersed in 0.1 M MES buffer (pH 5.5) containing 0.15 M EDC for 20 min then removed from EDC solution and immersed in 0.15 M NHS for other 20 min. The electrode was washed using MES buffer to remove unreacted EDC/NHS molecules. The modified and activated electrode was incubated with M13 phage solution (10^{11} PFU/mL) at 4 °C for 3–4 h, followed by rinsing with phosphate buffer (PB) solution to remove unbound phages. Subsequently, the electrode was immersed in 0.1 M ethanolamine solution for 30 min to passivate unreacted –NHS groups, followed by incubation with 0.2% BSA solution for 30 min to block unfunctionalized AuNPs. The electrode was washed thoroughly with PB solution. In this work, EA+BSA are labeled as "blocker" on graphs and schemes. All the modifications steps during the electrode fabrication were monitored and characterized using CV and EIS in ferricyanide solution.

2.5. Instruments and measurements

All electrochemical (CV and EIS) measurements were performed in potassium ferricyanide $K_3Fe(CN)_6$, as redox probe. The 10 mM ferricyanide solution was prepared in 0.1 M KCl and PB (pH 7.4). The electrochemical measurements were done using CHI 6005E electrochemical

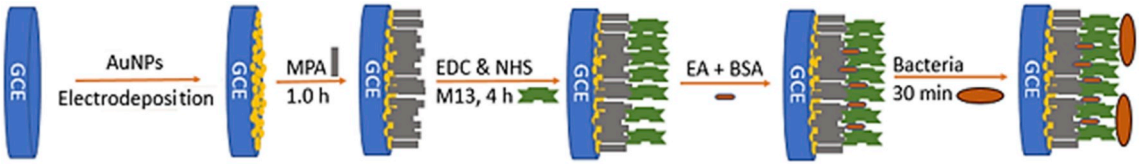

Fig. 1. Schematic diagram of the EIS cytosensor fabrication process.

work station (CH Instruments, Inc., Austin, Tx, USA) with Pt mesh as auxiliary electrode and Ag/AgCl as reference electrode. All EIS measurements were conducted at the Faradaic potential of 0.15 V, which was determined from CV ($E_{1/2} = 0.15$ V), and at the frequency range of 1–10^4 Hz. For detection of microbial cells, the modified and washed electrodes were immersed in bacterial cells suspension in PB at pH 7.4 for 30 min, washed to remove any non-specifically adsorbed bacterial cells, followed by EIS measurement. The charge transfer resistance value, R_{ct} (Ohms) was extracted by computer simulation and fitting of the data using the CHI 6005E software.

Charge transfer resistance change (ΔR_{ct}) is calculated from the equation $\Delta R_{ct} = R_{ctf}$ - R_{cti}, where R_{ctf} is the equilibrated R_{ct} after incubation with bacteria in PB or simulated river water followed by washing with PB, and R_{cti} is the recorded R_{ct} of the sensor after M13 immobilization and blocking, washing and incubation in PB or simulated river water followed by washing with PB.

The sensors were stored in refrigerator in PB, except for studies of temperature stability when they were stored at room temperature or 45 °C.

2.6. SEM imaging

The imaging was pursued on gold film instead of gold nanoparticles to avoid any feature overlapThe thin film of gold was functionalized with MPA and them modified with M13 phage and incubated with *E. coli XL1-Blue*. After 30 min incubation with *E. coli XL1-Blue*, the phage-modified electrode was rinsed with PB solution and left to dry for 2 h, and then coated with a thin film of Pt/Pd sputtering to enhance the conductivity of samples and avoid surface charging, as all phages, bacteria, EA and BSA are non-conductive.

2.7. Preparation of artificial water samples

The composition of the artificial river water was prepared to simulate the chemical/biological composition of Yamuna River in northern India. The samples were prepared by dissolving 50 mg/L sodium citrate, 60 mg/L ammonium chloride, 500 mg/L potassium chloride, 500 mg/L calcium chloride, and 150 mg/L magnesium nitrate in de-ionized water. The pH was adjusted to pH 7.5 and kept at 4 °C for future use. *E. coli XL1-blue* bacteria were spiked into an aliquot of the simulated river water samples and serially diluted to the required concentrations range (10^2–10^5 CFU/mL).

3. Results and discussion

As discussed in the introduction, the usage of bacteriophages as biorecognition elements in microbial biosensors is highly promising and preferred due to their higher stability compared to antibodies (Chen et al., 2015b). In addition, they are selective to their strains based on the receptors on the bacteria cell wall. The infection/binding process of M13 phage to *E. coli* involves the binding of the minor coat gene 3 protein (g3p) of the phage to the F pili (primary receptor) of bacteria, followed by the binding to the inner membrane protein TolA as a coreceptor (Bardhan et al., 2014; Karlsson et al., 2003; Lubkowski et al., 1999). Hence, it binds to *E. coli* strains with F^+, such as *XL1-Blue* and *K12*, while it doesn't bind to the non-*E. coli* strains. In this study, AuNPs were electrochemically deposited on the GCE to increase the available surface area and enhance the electron transfer at the electrodes surface. *E. coli XL1-Blue* and *K12* were used as the host/positive cells, while *P. chlororaphis* was implemented as the non-host/negative cells to test the EIS cytosensor selectivity. To eliminate potential false positive reading, the same measurements were carried out using a similar sensor structure but without modifying the sensor surface with M13 phage, as a control. To determine the efficiency of the EIS cytosensor, the sensitivity and LOD were determined using *XL1-Blue* as the host strain.

3.1. Cytosensor fabrication

3.1.1. Electrodeposition and characterization of AuNPs

As a clean, reproducible, and well dispersed particles-production method, electrochemical deposition was implemented to deposit a film of well dispersed AuNPs on the surface of GCE.

As mentioned in methods, the deposition was carried out using 15 cycles of CV in the potential range of −0.7 to −1.2 V, with a scan rate of 0.05 V/s (Elias et al., 2012). The CV of the GCE-AuNPs shows stronger redox peaks of ferricyanide compared to bare-GCE (Fig. 2a) which can be attributed to the higher surface area of AuNPs and their strong electrocatalytic activity (Chang et al., 2014). The EIS measurements were consistent with the CV measurement; as there is a clear decrease in the faradaic impedance response by introducing AuNPs (Fig. 2b). Moreover, SEM images showed good coverage of the GCE with well-dispersed and semi-spherical AuNPs (Fig. 2c). The average particle size was 51.64 ± 2.36 nm. EDX spectroscopy confirmed the successful formation of AuNPs, and the EDX mapping confirmed the NPs on the surface were AuNPs (Fig. 2d, e & 2f).

3.1.2. Bioreceptor functionalization and blocking

A robust and reproducible functionalization of electrode surface with bioreceptor and blockers is critical for a highly efficient biosensor. The success of each modification step in the cytosensor fabrication process was assessed by electrochemical techniques of CV and EIS using $[Fe(CN)_6]^{3-}$, as a redox probe. CV is a facile yet efficient technique for investigating modified electrode surface features. The deviations in peak current and peak potentials separation of redox probe are related to electron transfer rate constant. Fig. 3a illustrates the cyclic voltammograms post each functionalization/modification steps involved in the final sensor fabrication. As shown in the figure, there was a gradual decrease of the CV peak currents and correspondingly very small increase in the peak-to-peak redox potential after each modification. These changes are attributed to the repulsion of negatively charged $[Fe(CN)_6]^{3-}$ by –COOH groups of MPA and reduced conductivity of the electrode due to immobilization of non-conductive M13 phages and blocking with insulating BSA protein of GCE-AuNPs electrode.

EIS, another facile electrochemical technique which measures the electron transfer process at electrode-solution interface, was used to corroborate the above CV findings. The EIS measurements and corresponding Nyquist plots, shown in Fig. 3b, were fitted to Randles equivalent circuit, Fig. 3b **(inset)**, to calculate the charge transfer resistance (R_{ct}) after each modification step (Lisdat and Schäfer, 2008). Randles circuit is composed of the solution resistance (R_s), charge transfer resistance (R_{ct}) which is given by the diameter of the half-circle in the Nyquist plot, double layer capacitance (C_{dl}), and Warburg element (W). As anticipated and in agreement with CV results, R_{ct} increased after each modification confirming successful functionalization of the

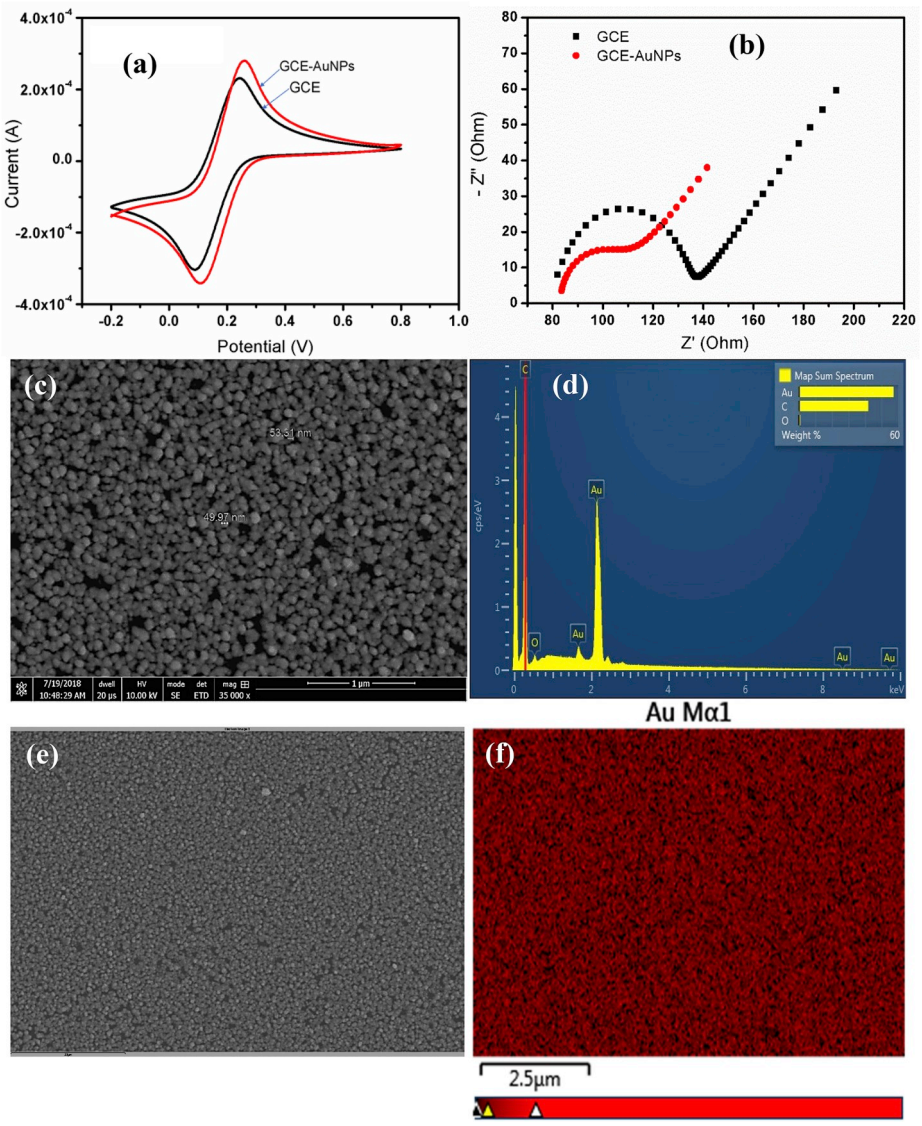

Fig. 2. Cyclic voltammograms (a) and Nyquist plots of EIS signal (b) of GCE and GCE-AuNP electrodes. SEM image (c), EDX (d) and EDX mapping (e and f) of electrodeposited AuNPs on GCE electrode.

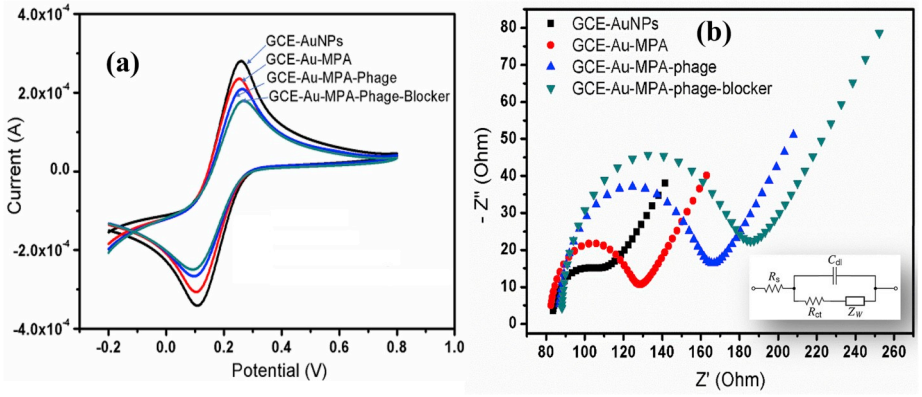

Fig. 3. Cyclic voltammograms (a) and Nyquist plots of the EIS responses (b) of GCE-AuNPs, GCE-Au-MPA, GCE-Au-MPA-phage and GCE-Au-MPA-phage-blocker electrodes. The inset is Randles equivalent circuit.

electrode surface with bioreceptor and blockers.

3.2. Optimization of incubation times of phages and target bacteria

To ensure highest loading efficiency of M13 phages on GCE-Au electrode, the electrode (GCE-Au-MPA-NHS) was incubated with 10^{11} PFU/mL solution of M13 for different time intervals (1, 2, 3, 4 & 8 h) and the corresponding ΔR_{ct} values were recorded. As illustrated in Fig. 4a, ΔR_{ct} gradually increased due to increased binding of M13 phages up to 3 h and then plateaued. In the same context, to determine the optimum incubation time of the analyte with the GCE-Au-MPA-NHS-M13-blocker electrode, 10^5 CFU/mL of *E. coli XL1-Blue* cells were incubated for 10, 20, 30 and 40 min. The results, Fig. 4b, showed an initial rapid increase in impedance due to the binding of a large number of *E. coli* cells followed by a slow increase and plateauing at 30 min.

Based on these results, a 3–4 h incubation time was used for phage immobilization and 30 min incubation of the phage-modified cytosensor with the analyte sample were employed in subsequent experiments.

3.3. Detection of E. coli XL1-Blue and E. coli K12

As mentioned above, detection of bacterial cells using M13 bacteriophage as a bioreceptor starts with the binding of the minor coat gene 3 protein (g3p) of M13 phage to the F pili (primary receptor) of bacteria, followed by binding to the inner membrane protein TolA as a coreceptor (Bardhan et al., 2014; Karlsson et al., 2003; Lubkowski et al., 1999). SEM imaging was performed to investigate the interaction between the bioreceptor M13 phage and its target *E. coli*. The SEM image in Fig. 5a shows nicely distributed clusters of the liquid crystal M13 phages on the gold surface with several captured *E. coli* cells (identified by red arrows). A zoomed-in image (Fig. 5b) of the captured bacteria shows phages surrounding the bacteria and immobilizing it to the electrode surface. A slightly enlarged/enveloped appearance of M13 phages may be attributed to the coating of PEG/NaCl, from the phage amplification process (please see methods) and/or a contribution from the blocker (0.2% BSA) as previously reported (Ploss and Kuhn, 2010; Sweeney et al., 2006).

It is worth briefly discussing the possible shapes and phases of M13 phages under different incubation/concentration conditions. M13 phages are liquid crystals of different phases. According to Dogic et al. (2016), at low concentrations, the phages are disordered and point in random directions in the isotropic phase. As the concentration increases, the phages start to be more oriented and aligned along one particular axis in the nematic phase that transitions to more ordered phases, particularly the smectic phase. Interestingly, phage molecules in the smectic phase organize into one-rod-length thick layers that are liquid-like aligned rods stacked on top of each other (Dogic et al., 2016). Moreover, M13 phage can have different shapes. It can be filamentous in the normal case, or spheroid in the hydrophobic-hydrophilic interfaces, or I-form particles at low temperatures (around 2 °C) (Manning et al., 1981; Ngo-Duc et al., 2014).

3.4. Analytical characteristics of the cytosensor

We evaluated the performance of the cytosensor in terms of sensitivity, limit of detection, reproducibility and selectivity. Fig. 6 shows the sensor response (ΔR_{ct}) as a function of *E. coli XL1-Blue* concentration. The results showed that the cytosensor response (ΔR_{ct}) increased, i.e. R_{ct} increased, as a function of *E. coli XL1-Blue* concentration over a broad dynamic range from 10^1 to 10^7 CFU/mL (Fig. S1). The calibration plot in Fig. 6 is an average of responses of three separate cytosensors with each sensor exposed to 10-fold increasing concentrations of the target bacteria covering the 10^1–10^7 CFU/mL range. Each analyte sample was incubated with the cytosensor for 30 min, washed with PB followed by EIS measurement in between the samples. The increase in charge transfer resistance can be attributed to the insulating effect of the bacterial cells, and the possibility that they prevent redox probe molecules from reaching the electrode surface (Bekir et al., 2015; Tlili et al., 2013).

The positive control experiment, in which the sensor without M13 phage was exposed to 10^3, 10^4 and 10^5 CFU/mL of *E. coli XL1-Blue* had a minimal response when compared to a sensor with bioreceptor M13 phage (Fig. S2, see Supplementary information). Additionally, negative control experiment in which a cytosensor with M13 phage was exposed to blank PB, i.e. no *E. coli XL1-Blue*, repeatedly had a response of $\Delta R_{ct} = 4.00 \pm 3.51$ (n = 3). The above results confirmed the high quality of biofunctionalization protocol and the corresponding cytosensors prepared in this study.

3.4.1. Sensitivity and limit of detection

As shown in Fig. 6, the cytosensor response was linearly related to the log of *E. coli XL1-Blue* concentration between 10^1 to 10^5 CFU/mL with a sensitivity (the slope of the calibration plot, d(ΔRct)/dlog(CFU/mL)) of 7.78 Ohms per Log (CFU/mL) or 7.78 Ohms per 10 (CFU/mL). The limit of detection (LOD) of the cytosensor calculated based on the equation LOD = 3*Sd/S, where Sd is the standard deviation of blank sample (SD = 3.51 Ohms, n = 3), and S is the sensitivity, was estimated to be 13.53 ≈ 14 CFU/mL. This limit of detection is the lowest in the EIS-phage cytosensors published to-date (Bekir et al., 2015; Han et al., 2016; Li et al., 2014; Shabani et al., 2013; Tlili et al., 2013; Zhou et al., 2017). This low LOD may be credited to 1) the non-lytic nature of the M13 phages which helped detect bacterial cells as an increase in Rct, without getting countered by the conductive content of cells released from the cells, as in the case of lytic phages based biosensors and 2) the high surface area of AuNPs and the efficient chemical binding of M13 to the nanoparticles surface. Furthermore, the cytosensors had excellent

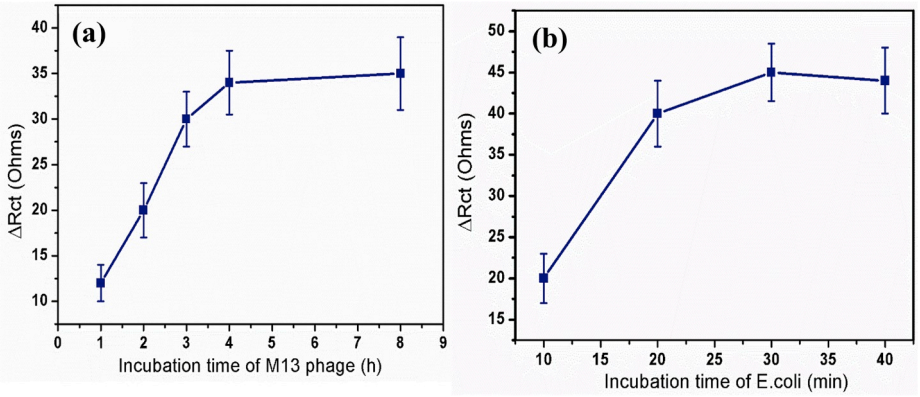

Fig. 4. Optimization of the incubation times of (a) M13 phages with GCE-AuNP-NHS and (b) E. coli XL1-Blue (10^5 CFU/mL) cells with the GCE-Au-MPA-phage-blocker electrodes. Each data point is an average of responses from 1 electrode, measured 3 times and error bars represent ±1 standard deviation. (For interpretation of the references to colour in this figure legend, the reader is referred to the Web version of this article.)

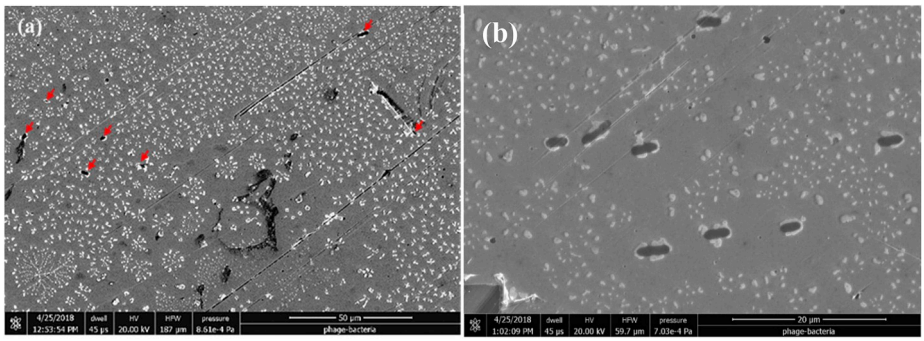

Fig. 5. (a) SEM micrograph of the M13 phages immobilized on Au electrode and captured *E. coli XL1-Blue* cells (pointed at by red arrows). (b) Higher magnification SEM image of *E. coli* bacteria captured by M13 phages. (For interpretation of the references to colour in this figure legend, the reader is referred to the Web version of this article.)

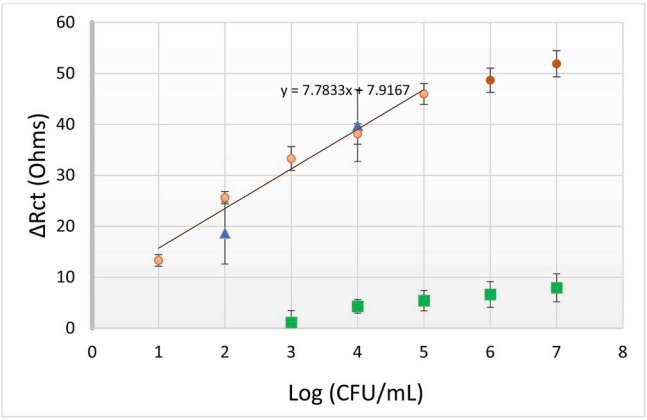

Fig. 6. Response (ΔR_{ct}) of the cytosenor to increasing concentrations of *E. coli XL1-Blue* (circles); *E. coli* K-12 (triangles) and *P. chlororaphis* (squares). Each data point is an average of responses from 3 different M13-modified electrodes and error bars represent ±1 standard deviation. (For interpretation of the references to colour in this figure legend, the reader is referred to the Web version of this article.)

reproducibility as evident by the low standard deviation (1.12 to 2.57) and relative standard deviation (4.46–8.47%; please see Table S1 in Supplementary Information) of the data points obtained from 3 independent cytosensors used to generate the calibration plot in Fig. 6.

3.4.2. Selectivity

Similar to *E. coli XL1-Blue*, *E. coli K12* is F pili positive and host for M13 phages. Therefore, an increase in impedance is expected after incubation of the M13-modified sensor with this strain also. As shown in Fig. S3, there was an increase in half-circle diameter of Nyquist plot, which represents the charge transfer resistance of cytosensor from the original value when exposed to 10^2 and 10^4 CFU/mL of *E. coli K12*. The ΔR_{ct} values for these concentrations were statistically similar to that for *E. coli XL1-Blue* (Fig. 6). On-the-other-hand, as shown in Fig. 6, there was no significant change in the charge transfer resistance with the non-host *P. chlororaphis* bacteria (ΔR_{ct} values were similar to that for blank/buffer even at 10^7 CFU/mL) compared to the response with the host *E. coli XL1-Blue*. The ability of our sensor to detect multiple strains of *E. coli* while not responding to non-*E. coli* bacteria, is a useful characteristic in the goal of selectively monitoring coliforms.

3.4.3. Stability

The M13 phage-based EIS cytosensor was tested for stability at 22 °C (room temperature) and 45 °C by comparing ΔRct for detection of *E. coli XL-1 blue* at the same concentration (10^3 CFU/mL). Fourteen M13 phage modified cytosensors, were prepared on working electrodes of evaporated gold on Kapton substrate that was modified with M13 phage and blocked with blocking agents using protocol described previously. A pair of sensors were used immediately for the day zero time point reading while six sensors each were kept in PB at 22 °C (room temperature) and 45 °C until day 16 for future time points. Two electrodes were removed from each storage condition and evaluated for detection efficiency. As shown in Table S2, there was no significant difference in the sensing efficiency of the sensors for up to 16 days at these temperatures. The stability at temperature as high as 45 °C for an extended period is a beneficial feature of our phage-based sensor over antibodies-based sensors for field applications and variation of temperature that the sensor may encounter during shipping. Additionally, the stability of the M13-based EIS sensor was investigated in a wide range of pH values. Multiple electrodes were prepared the same way as mentioned earlier and incubated in pH 2.0 to 10.0 buffer for an hour followed by evaluating detection of 10^3 CFU/mL *E. coli XL-1 blue* in PB. As illustrated in Fig. S4, the sensor had negligible decrease in sensing response over the pH range of 4.5–8.0, that decreased slightly to 80 ± 14% at pH 10 and 75 ± 20% at pH 3 and dropped significantly to 35 ± 10% at pH 2. These results verify the very good to high stability of M13 phage-based sensor on exposure to pH 3 to 10.

3.5. Analysis of simulated river water samples

To assess the suitability of M13 phage-based EIS cytosensor for practical application, it was applied to detect *E. coli XL1-Blue* spiked in simulated river water mimicking the chemical/biological composition of Yamuna River in northern India. The sensor response in river water was compared to that in PB for bacteria concentration from 10^2 to10^5 CFU/mL. As shown in Fig. 7, the response was linearly correlated to the concentration over this concentration range with a slope of 6.685 Ohms per 10 CFU/mL, which was statistically identical ($p > 0.05$) to that in PB (S = 6.583 Ohms per 10 CFU/mL) over all the concentrations. A slight consistent off-set/difference of the sensor response between simulated river water and PB can be attributed to the difference in composition of the two water samples. These results demonstrate the promise of the present sensor for the real field applications.

4. Conclusions

To conclude, an easy to fabricate and use EIS cytosensor based on non-lytic bacteriophage M13 for measurement of coliforms was introduced. The sensor exhibited the lowest limit of detection (≈14 CFU/mL) reported to-date for phage-based EIS cytosensors for coliforms. This excellent limit of detection of the cytosensor can be attributed to the non-lytic nature of the M13 phage, the high surface area of AuNPs, and the efficient chemical binding of M13 to the surface of well-dispersed nanoparticles. The sensor was selective for F^+ pili *E. coli* species, such as *XL1-Blue and K12*, when compared to non-host *P. chlororaphis*

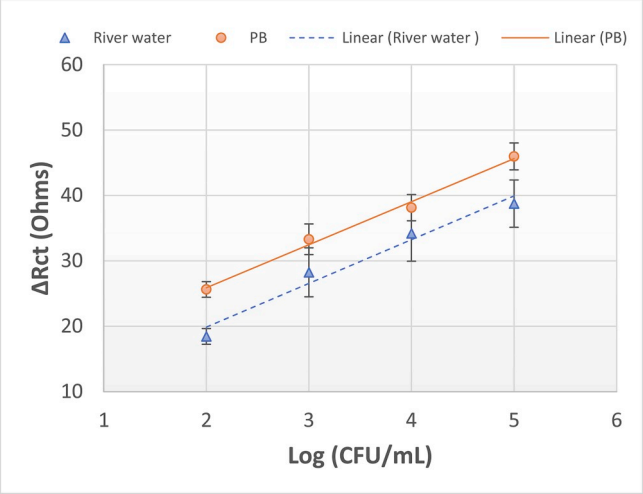

Fig. 7. Response (ΔR_{ct}) of the cytosenor to increasing concentrations of *E. coli XL1-Blue* in PB (circle) and simulated river water (square). Each data point is an average of responses from 1 electrode, measured 3 times and error bars represent ±1 standard deviation. (For interpretation of the references to colour in this figure legend, the reader is referred to the Web version of this article.)

bacteria. In terms of its suitability to real field application, the M13 sensor system was tested in simulated river water, where it exhibited good response with neglectable interference with the water composition variation. These features make it a potential analytical tool ideal for monitoring coliform in environmental waters. In addition, the sensor system shows high stability over a wide range of pH and at elevated temperatures. Summing all together, the proposed M13 phage-based cytosensor is highly sensitive, selective, and stable for detection of fecal coliforms in water samples.

Declaration of competing interest

The authors declare that they have no known competing financial interests or personal relationships that could have appeared to influence the work reported in this paper.

CRediT authorship contribution statement

Mohammed Sedki: Conceptualization, Methodology, Formal analysis, Investigation, Writing - original draft, Writing - review & editing, Visualization. **Xingyu Chen:** Investigation. **Chuan Chen:** Resources. **Xin Ge:** Resources, Supervision, Writing - review & editing. **Ashok Mulchandani:** Conceptualization, Methodology, Resources, Writing - review & editing, Supervision, Project administration, Funding acquisition.

Acknowledgements

This work was supported by a grant from the DST/Intel®/Indo-U.S. Science and Technology Forum (RP03472). AM acknowledges the financial support of W. Ruel Johnson Chair.

Appendix A. Supplementary data

Supplementary data to this article can be found online at https://doi.org/10.1016/j.bios.2019.111794.

References

Ashbolt, N.J., Grabow, W.O.K., Snozzi, M., 2001. IWA Publishing, London, pp. 289–315 (Chapter 13).
Bao, C., Chen, L., Wang, T., Lei, C., Tian, F., Cui, D., Zhou, Y., 2013. Nano-Micro Lett. 5, 213–222.
Bardhan, N.M., Ghosh, D., Belcher, A.M., 2014. J. Biophot. 7, 617–623.
Bekir, K., Barhoumi, H., Braiek, M., Chrouda, A., Zine, N., Abid, N., Maaref, A., Bakhrouf, A., Ouada, H. Ben, Jaffrezic-Renault, N., 2015. Environ. Sci. Pollut. Res. 22, 15796–15803.
Burnham, S., Hu, J., Anany, H., Brovko, L., Deiss, F., Derda, R., Griffiths, M.W., 2014. Anal. Bioanal. Chem. 406, 5685–5693.
Byrne, B., Stack, E., Gilmartin, N., O'Kennedy, R., 2009. Sensors 9, 4407–4445.
Chang, G., Shu, H., Ji, K., Oyama, M., Liu, X., He, Y., 2014. Appl. Surf. Sci. 288, 524–529.
Chen, J., Alcaine, S.D., Jiang, Z., Rotello, V.M., Nugen, S.R., 2015. Anal. Chem. 87, 8977–8984.
Chen, J., Duncan, B., Wang, Z., Wang, L.-S., Rotello, V.M., Nugen, S.R., 2015. Nanoscale 7, 16230–16236.
Dogic, Z., 2016. Front. Microbiol. 7, 1013.
Dye, C., 2014. Phil. Trans. R. Soc. B 369, 20130426.
Edgar, R., McKinstry, M., Hwang, J., Oppenheim, A.B., Fekete, R.A., Giulian, G., Merril, C., Nagashima, K., Adhya, S., 2006. Proc. Natl. Acad. Sci. 103, 4841–4845.
Elias, J., Gizowska, M., Brodard, P., Widmer, R., Graule, T., Michler, J., Philippe, L., 2012. Nanotechnology 23, 255705.
Ertürk, G., Lood, R., 2018. Sens. Actuators B Chem. 258, 535–543.
Guo, X., Kulkarni, A., Doepke, A., Halsall, H.B., Iyer, S., Heineman, W.R., 2011. Anal. Chem. 84, 241–246.
Han, L., Liu, P., Petrenko, V.A., Liu, A.H., 2016. Sci. Rep. 6, 1–10.
Handa, H., Gurczynski, S., Jackson, M.P., Auner, G., Walker, J., Mao, G., 2008. Surf. Sci. 602, 1392–1400.
Hassan, R.Y.A., Wollenberger, U., 2016. Anal. Bioanal. Chem. 408, 579–587.
Ivnitski, D., Abdel-Hamid, I., Atanasov, P., Wilkins, E., Stricker, S., 2000. An Int. J. Devoted to Fundam. Pract. Asp. Electroanal. 12, 317–325.
Janczuk, M., Niedziółka-Jönsson, J., Szot-Karpińska, K., 2016. J. Electroanal. Chem. 779, 207–219.
Karlsson, F., Borrebaeck, C.A.K., Nilsson, N., Malmborg-Hager, A.-C., 2003. J. Bacteriol. 185, 2628–2634.
Keer, J.T., Birch, L., 2003. J. Microbiol. Methods 53, 175–183.
Li, Y., Afrasiabi, R., Fathi, F., Wang, N., Xiang, C., Love, R., She, Z., Kraatz, H.-B., 2014. Biosens. Bioelectron. 58, 193–199.
Lim, D.V., Simpson, J.M., Kearns, E.A., Kramer, M.F., 2005. Clin. Microbiol. Rev. 18, 583–607.
Lisdat, F., Schäfer, D., 2008. Anal. Bioanal. Chem. 391, 1555.
Lubkowski, J., Hennecke, F., Plückthun, A., Wlodawer, A., 1999. Structure 7, 711–722.
Manning, M., Chrysogelos, S., Griffith, J., 1981. J. Virol. 40, 912–919.
Massad-Ivanir, N., Shtenberg, G., Raz, N., Gazenbeek, C., Budding, D., Bos, M.P., Segal, E., 2016. Sci. Rep. 6, 38099.
Nanduri, V., Sorokulova, I.B., Samoylov, A.M., Simonian, A.L., Petrenko, V.A., Vodyanoy, V., 2007. Biosens. Bioelectron. 22, 986–992.
Neufeld, T., Schwartz-Mittelmann, A., Biran, D., Ron, E.Z., Rishpon, J., 2003. Anal. Chem. 75, 580–585.
Ngo-Duc, T.-T., Zaman, M.S., Moon, C.-H., Haberer, E.D., 2014. International Society for Optics and Photonics, p. 91710X.
Odonkor, S.T., Ampofo, J.K., 2013. Microbiol. Res. (Pavia). 4, 2.
Ploss, M., Kuhn, A., 2010. Phys. Biol. 7, 45002.
Rawson, F.J., Downard, A.J., Baronian, K.H., 2014. Sci. Rep. 4, 5216.
Sedki, M., Hassan, R.Y.A., Hefnawy, A., El-Sherbiny, I.M., 2017. Sens. Actuators B Chem. 252 https://doi.org/10.1016/j.snb.2017.05.163.
Selim, H.M.M., Kamal, A.M., Ali, D.M.M., Hassan, R.Y.A., 2017. Electroanalysis 29, 1498–1505.
Setterington, E.B., Alocilja, E.C., 2012. Biosensors 2, 15–31.
Shabani, A., Marquette, C.A., Mandeville, R., Lawrence, M.F., 2013. Analyst 138, 1434–1440.
Soper, S.A., Henry, A.C., Vaidya, B., Galloway, M., Wabuyele, M., McCarley, R.L., 2002. Anal. Chim. Acta 470, 87–99.
Spiegelman, D., Whissell, G., Greer, C.W., 2005. Can. J. Microbiol. 51, 355–386.
Sweeney, R.Y., Park, E.Y., Iverson, B.L., Georgiou, G., 2006. Biotechnol. Bioeng. 95, 539–545.
Tlili, C., Sokullu, E., Safavieh, M., Tolba, M., Ahmed, M.U., Zourob, M., 2013. Anal. Chem. 85, 4893–4901.
von Wintzingerode, F., Göbel, U.B., Stackebrandt, E., 1997. FEMS Microbiol. Rev. 21, 213–229.
Wallace, D.C., Fan, W., Procaccio, V., 2010. Annu. Rev. Pathol. Mech. Dis 5, 297–348.
Wibowo, K.M., Sahdan, M.Z., Ramli, N.I., Muslihati, A., Rosni, N., Tsen, V.H., Saim, H., Ahmad, S.A., Sari, Y., Mansor, Z., 2018. J. Phys. Conf. Ser. 12063. IOP Publishing.
Zhang, A., Guo, W., Ke, H., Zhang, X., Zhang, H., Huang, C., Yang, D., Jia, N., Biosens. Bioelectron. 101, 219–226.
Zhou, Y., Marar, A., Kner, P., Ramasamy, R.P., 2017. Anal. Chem. 89, 5734–5741.